ACS OMEGA

http://pubs.acs.org/journal/acsodf

Article

Facile Synthesis of NiO−CuO/Activated Carbon Nanocomposites for Use in the Removal of Lead and Cadmium Ions from Water

Bara'ah Yahya Hashem, Abdullah A. Alswat, Shaimaa L. Ali, Najat A. Al-Odaini, and Fares T. Alshorifi*

Cite This: *ACS Omega* 2022, 7, 47183−47191

Read Online

ACCESS | Metrics & More | Article Recommendations

ABSTRACT: In this work, activated carbon (AC) was synthesized and then modified using nickel(II) oxide and copper(II) oxide. Pure-AC, 10, 20, 30, and 40 wt % nanohybrid NiO−CuO/AC nanocomposites (χ-NC/AC NCs) were characterized using XRD, IR, EDS, surface area, and FE-SEM techniques. Furthermore, the adsorbents obtained were tested for their ability to remove hazardous Pb(II) and Cd(II) from water. The fabricated *x*-NC/AC NC adsorbents showed the highest adsorptive performance toward the adsorption of Pb(II) and Cd(II) from water. The 30-NC/AC NC adsorbent showed the complete removal of Pb(II) at pH = 5 and Cd(II) at pH = 7 within 30 min. Overall, the obtained superior experimental results suggest that the adsorptive performance of AC was greatly enhanced after loading hybrid metal oxide nanoparticles, so its application in water treatment is potential and applicable.

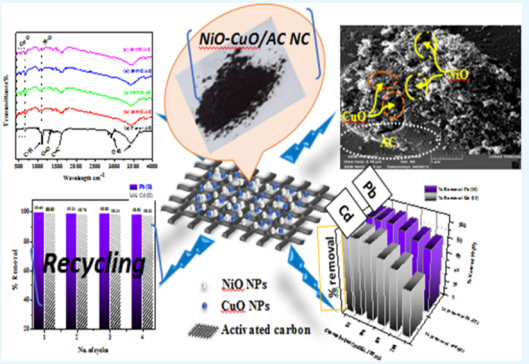

1. INTRODUCTION

Nowadays, a green and clean environment is considered one of the hottest topics in academia and industry.[1] Heavy-metal wastewater is increasingly being discharged into the environment from different industries.[2] What is more, they are the most abundant elements in the earth's crust, and they can only be transformed into nontoxic forms rather than biodegradable ones. Large amounts of such metals can be toxic or fatal to all forms of life, including microorganisms, plants, animals, and humans.[3] Metal concentrations that accumulate in soil have a negative impact on productivity and fertility.[4] The accumulation of lethal heavy metals in our bodies has serious health consequences, including growth and developmental abnormalities, mental illnesses, and metabolic failure.[5] The toxicity of cadmium [Cd(II)] is a significant issue in some countries.[6−9] Heavy Cd(II) ions are environmentally toxic heavy-metal ions that harm all biological functions in plants, animals, and humans, so it was ranked seventh by the agency for toxic substances and disease registry.[6,7] As a result, it mimics various elements, causing disruption and alteration at various levels of the ecosystem.[10] Lead [Pb(II)] has the potential to harm the human/animal nervous system, kidneys, liver, brain functions, and reproductive system,[11] and it also leads to some other toxic symptoms such as headache, muscle weakness, anemia, insomnia, dizziness, irritability, and hallucination.[12] To protect our environment and health, these toxic metallic ions should be removed from polluted drinking water using different water treatment methods.[13] Among them is the adsorption method as a quick and general method for efficiently and affordably removing toxic metal ions from polluted drinking water. Various solid adsorbents such as zeolites and polymeric materials have been used. Carbon-based adsorbents such as modified activated carbon (AC) and other carbonic materials (graphene oxide and carbon nanotubes) have received a lot of attention recently because of their high thermal and chemical stability.[14] AC is the most commonly used adsorbent which is characterized by low cost, a large surface area, high thermal and chemical stability, high porosity, and a controllable pore size distribution.[15] However, an AC adsorbent lacks functional groups, so its use in heavy-metal ion adsorption has been limited due to its low uptake and slow kinetics.[16] Because of the transition-metal oxides' role in photocatalytic degradation, adsorption, metallurgy, chemical catalysis, and high-temperature superconductors process, NiO and CuO nanoparticles (NPs) with/without support have been reported for many years using several preparation methods.[17−20] A significant effort is currently being made to investigate the potential applications of metal oxide NPs supported to develop their adsorption capacities. Nanocomposites (NCs) of iron oxide with AC in various w/w ratios were prepared and tested for Cr(VI) removal using the coprecipitation technique.[21,22] The NC is free from the environmentally toxic polyvalent ions present in other neat metallic nanoadsorbents.[21] Jain et al.

Received: October 1, 2022
Accepted: November 23, 2022
Published: December 7, 2022

ACS Publications

© 2022 The Authors. Published by American Chemical Society

https://doi.org/10.1021/acsomega.2c06352
ACS Omega 2022, 7, 47183−47191

reported the synthesis of magnetic-Fe_3O_4 NPs and magnetic-Fe_3O_4/AC NCs in batch mode for the adsorption of heavy Cu, Cd, and Cr ions.[22] The Kakavandi group[23] investigated Pb(II) adsorption on a magnetic-Fe_3O_4/AC composite. Similarly, Kumar et al. successfully prepared ZnO/AC NC adsorbents with an adsorptive capacity of 96.15 mg/g for Cd(II) ions in aqueous solutions.[24] Apart from that, CuO/AC NCs and NiO/AC NCs were reported for supercapacitor electrode application and electrocatalytic oxidation of phenol, respectively.[25,26] However, to the author's best knowledge, no publications are available in the literature that addresses hybrid NiO−CuO/AC NCs for the removal of Cd(II) and Pb(II) from water. This article introduces a new series of nanohybrid NiO−CuO/AC NCs (*x*-NC/AC NCs) as efficient solid nanoadsorbents for obtaining a complete removal of toxic Cd(II) and Pb(II) from polluted drinking water. Batch experiments were carried out to evaluate the adsorptive performance of pure-AC and fabricated *x*-NC/AC NC adsorbents and their recycling. Using atomic absorbance spectroscopy, the Cd^{2+} and Pb^{2+} in the batch experiments were quantified both before and after adsorption. AC and *x*-NC/AC NC adsorbents were characterized using X-ray diffraction (XRD), infrared (IR) spectroscopy, energy-dispersive X-ray spectroscopy (EDS), N_2 adsorption/desorption isotherm [Brunauer−Emmett−Teller (BET) surface area], and field emission scanning electron microscopy (FE-SEM) techniques.

2. EXPERIMENTAL SECTION

2.1. Chemical Reagents. Arhabi-Khat leaves were picked up in the Arhab region, Sana'a, Republic of Yemen. Sigma-Aldrich provided all chemicals and reagents used in this study, including Ni $(NO_3)_2{\cdot}6\ H_2O$ (98%), Cu $(NO_3)_2{\cdot}6\ H_2O$ (98%), NaOH (98%), KOH (99%), HCl (37%), $PbCl_2$ (99.99%), and $HgCl_2$ (99%). Distilled water (D. W.) was obtainedfrom our lab.

2.2. Synthesis of Ac and *x*-NC/AC NC Adsorbents. AC was synthesized from Arhabi-Khat leaves as a plant source using a 2.0 N KOH solution and heated at 400 °C for 4 h. The washed, crushed, sifted, and dried powdered Khat (60 g) was soaked in KOH (2.0 N/500 mL) overnight. The filtered blackish-wet carbonic solid was washed several times with 0.1 M HCl and D. W. until obtaining the neutral pH level of the wet carbonic solid. The dried and washed black-carbonic solid was then heated for 4 h at 400 °C. The *x*-NC/AC NCs were fabricated with different mass percentages (10−40 wt %) of NiO−CuO loaded on AC power. Typically, 2.0 g of AC powder was dispersed in 80 mL of D. W. under ultrasonication. An appropriate amount of Cu $(NO_3)_2{\cdot}6\ H_2O$ and Ni $(NO_3)_2{\cdot}6\ H_2O$ (in equal molar ratios) was dissolved separately in 20 mL of D. W. and then added to the AC/H_2O suspension with stirring for 20 min. 2.0 M NaOH solution was added dropwise to the metal ions' AC suspension until the pH level was 11, with stirring for 30 min, and then heated at 150 °C in an autoclave for 2 h. The dried washed and filtered *x*-NC/AC NCs were separately calcined at 400 °C for 4 h. The prepared AC, 10, 20, 30, and 40 wt % NC/AC NC adsorbents were labeled as AC, 10-NC/AC NC, 20-NC/AC NC, 30-NC/AC NC, and 40-NC/AC NC adsorbents, respectively.

2.3. Characterization Techniques. The surface chemistry and morphology of AC, 10-NC/AC NC, 20-NC/AC NC, 30-NC/AC NC, and 40-NC/AC NC adsorbents were characterized using XRD (Shimadzu XRD model 6000, Japan), a field emission scanning electron microscope (JOEL JSM 7600, set to 5 kV) equipped with an energy-dispersive X-ray spectrometer (Oxford Instruments) [Fourier transform infrared (FT-IR), 100 Perkin Elmer FT-IR 1650 spectrophotometer]. Micrometrics (USA) ASAP2020 volumetric instrument was used to measure nitrogen adsorption−desorption isotherms. The concentrations of lead and mercury were determined using flame emission atomic absorption spectroscopy (Thermo Scientific, S series).

3. RESULTS AND DISCUSSION

As mentioned previously, this work aimed to synthesize a new series of *x*-NC/AC NCs as efficient adsorbents for the removal of toxic Cd(II) and Pb(II) from water. Fabricated nanohybrid NiO−CuO/AC NC adsorbents were characterized using various techniques such as XRD, FT-IR, EDS, N_2 adsorption/desorption isotherm (BET surface area), and FE-SEM. In this section, the results are divided into two parts as follows.

3.1. Morphological Studies. Figure 1 outlines the FT-IR bands of neat-AC, 10-NC/AC NC, 20-NC/AC NC, 30-NC/

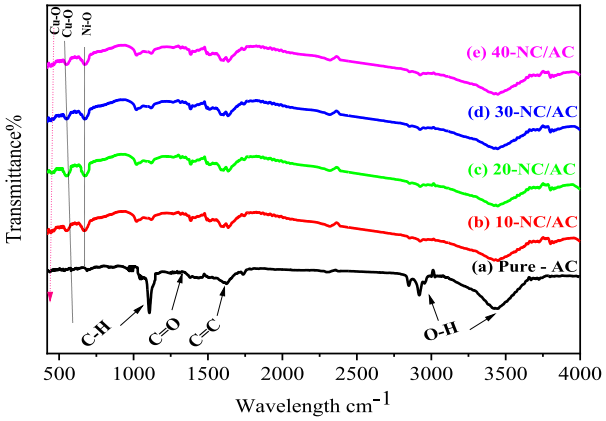

Figure 1. FT-IR spectra of (a) pure-AC (b) 10-NC/AC NC, (c) 20-NC/AC NC, (d) 30-NC/AC NC, (e) and 40-NC/AC NC samples.

AC NC, and 40-NC/AC NC samples discovered in all the fabricated *x*-NC/AC NCs. The broad absorption bands at about 3375 and 1616 cm^{-1} are appointed to OH-groups of absorbed-H_2O molecules and the AC C═C stretching, respectively. The FT-IR bands at (1397, 1747), (1356/1242), (1112−1029), 963, 846, and 804 cm^{-1} correspond to (C═O, carbonyl/carboxyl group), (CH_2 symmetric bending/twisting), (C−O−C, C−O stretching), (out-of-plane rings C−H bending), (C−H out-plane bends aromatic ring), and (C−C stretching vibrations), respectively. The FT-IR spectra of 10-NC/AC NC, 20-NC/AC NC, 30 NC/AC NC, and 40-NC/AC NC samples revealed new FT-IR bands in comparison to the pure-AC sample; Ni−O stretching and bending modes were indicated at 676 cm^{-1}.[27,28] The FT-IR bands obtained at 468 and 524 cm^{-1} correspond to Cu−O bond vibration.[29] The bands appearing in the FT-IR spectra of *x*-NC/AC NCs clearly confirmed the formation of *x*-NC/AC NCs. The chemical formation of *x*-NC/AC NCs is also confirmed by XRD and EDX later.

Powder XRD patterns confirmed the crystalline chemical structure and purity of the synthesized *x*-NC/AC NCs. Figure 2 depicts two diffraction peaks of amorphous AC at 2θ = 23.5 and 43.5°, corresponding to the (002) and (100) index planes.[26] In addition, the peaks at 2θ = 37.1, 43.2, 62.7, and

https://doi.org/10.1021/acsomega.2c06352
ACS Omega 2022, 7, 47183−47191

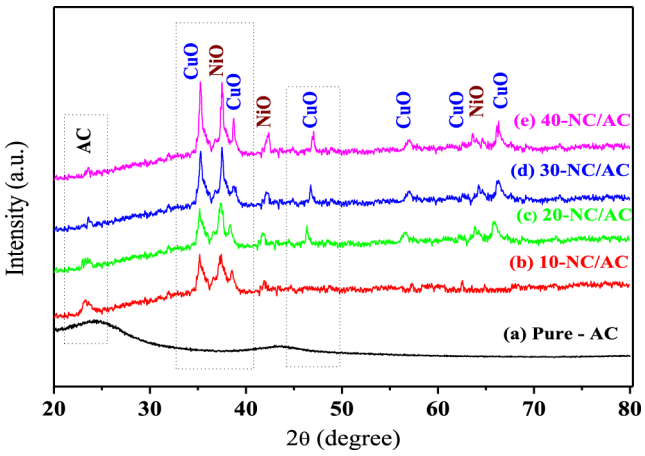

Figure 2. XRD patterns of (a) pure-AC, (b) 10-NC/AC NC, (c) 20-NC/AC NC, (d) 30-NC/AC NC, and (e) 40-NC/AC NC samples.

75.3° are assigned to the (111), (200), (220), and (311) planes indicating cubic crystalline NiO NPs (CPDS no. 71-1179).[30] Moreover, the XRD pattern revealed also several peaks, confirming the monoclinic crystalline CuO nature. These XRD peaks appeared at 2θ = 32.60, 35.78, 38.95, 48.88, 53.55, 58.42, 61.79, 66.65, 68.33, 68.33, 72.45, and 75.10° with their respective indices corresponding to the (110), (111), (200), (202), (020), (202), (113), (310), (220), (311), and (222) planes (JCPDS PDF file no. 89-5895).[30] This XRD pattern of *x*-NC/AC NC samples confirmed that *x*-NC/AC NCs had a mixed nature of NiO, CuO, and AC NPs. Overall, the XRD peaks illustrate that hybrid NiO−CuO NPs were successfully loaded on the AC surface, without any effect on their phase and crystal structure. The NiO−CuO and AC peak (at 2θ = 43.1) overlapped, which led to a reduction in AC-XRD intensity due to the formation of x-NC/AC NC samples, so the AC pattern is not recognizable by the naked eye because of the high intensity of NiO−CuO peaks. The crystallite sizes of hybrid NiO−CuO NPs were between 30 and 45 nm. The chemical formation of *x*-NC/AC NCs is also confirmed by FT-IR spectroscopy and EDX. The sizes and distribution of nanohybrid NiO−CuO in all *x*-NC/AC NCs will be confirmed by FE-SEM later.

FE-SEM was used to investigate the morphology and microstructural properties of fabricated *x*-NC/AC NCs. Figure 3a−d shows the FE-SEM images of 10, 20, 30, and 40-NC/AC NC samples at higher magnification. The FE-SEM images show that *x*-NC/AC NC samples are composed of a high-density and compact arrangement of homogeneous small spherical granules with a wide distribution on the AC surfaces, indicating spherical NiO−CuO NPs loaded on AC surfaces. Along with their extremely small dimensions, the FE-SEM image of the 40-NC/AC NC adsorbent showed also that some of the small particles aggregate to form secondary particles; therefore, it was observed that some clumps formed on its surfaces. The FE-SEM results indicate that nanohybrid NiO−CuO particles loaded successfully on the AC surface. The effective atomic concentrations of the elements of *x*-NC/AC NC adsorbents are outlined in the EDS of pure-AC and 30-NC/AC NC samples. The EDS spectra of *x*-NC/AC NCs confirmed the presence of C (at 0.25 keV), O (at 0.523 keV), Cu (at 1.486 and 8.04 keV), and Ni (at 1.486, 6.391, and 7.471 keV). The C, O, Cu, and Ni compositions in the 30-NC/AC NC sample are shown in the table inset in Figure 4.

The surface properties of the synthesized AC and *x*-NC/AC NCs were investigated using nitrogen adsorption/desorption measurements. Figure 5 depicts the nitrogen sorption isotherms and pore size distributions of the *x*-NC/AC NCs samples. According to N_2 adsorption/desorption, the fabricated *x*-NC/AC NC adsorbents had type IV H 4 hysteresis, which was also a direct indication of the presence of mesopores (diameter 2−50 nm).[31] Neat-AC, 10-NC/AC NC, 20-NC/AC NC, 30-NC/AC NC, and 40-NC/AC NC samples had BET surface areas of 484.25, 461.04, 447.01, 421.00, and 370.80 m^2/g, respectively. Because of the highly mesoporous AC

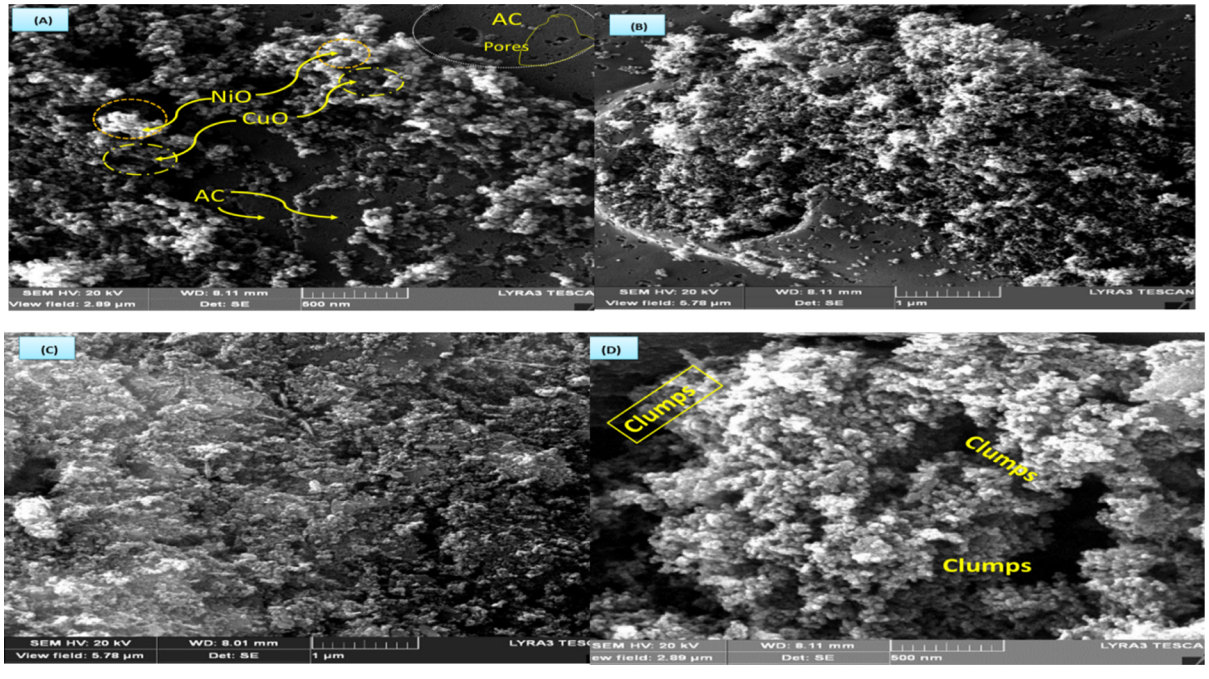

Figure 3. FE-SEM images of (a) 10-NC/AC NC, (b) 20-NC/AC NC, (c) 30-NC/AC NC, and (d) 40-NC/AC NC samples.

https://doi.org/10.1021/acsomega.2c06352
ACS Omega 2022, 7, 47183−47191

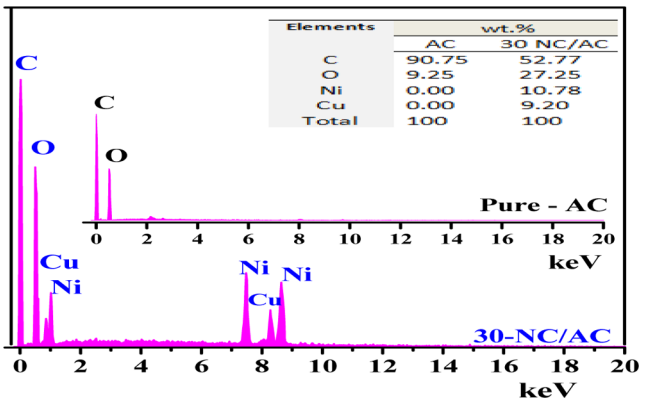

Figure 4. EDS pattern of pure-AC and 30-NC/AC NC samples.

nature, the pure-AC adsorbent had a larger surface area than all *x*-NC/AC NC adsorbents. The highest specific surface area of pure-AC adsorbent indicates that AC has the potential to be appropriate support for bonding with metal oxides. Besides, the surface area of *x*-NC/AC NC adsorbents decreased along with increasing loaded nanohybrid NiO−CuO content, which possibly confirmed the successful loading and formation of hybrid NiO−CuO NPs onto the AC structure, leading to the blockage of some mesopores of the AC structure and reduction in the pore diameter and volume. The total pore volume is a measure of the total porosity of the solid nanoadsorbents. The % porosity was 58.57, 61.78, 47.05, 37.96, and 23.30% for neat-AC, 10-NC/AC NC, 20-NC/AC NC, 30-NC/AC NC, and 40-NC/AC NC adsorbents. Thus, the used *x*-NC/AC NC adsorbents are of interest as possible materials to be used in water purification. The % porosity decreased after loading of the 20, 30, and 40 wt % NiO−CuO NPs, and as the loaded NiO−CuO amount increased, the porosity of the adsorbent decreased; this may be due to the deposition of the hybrid metal oxides in the AC pores.

3.2. Application. *3.2.1. Effect of Solution pH.* Figure 6 depicts the effect of testing four pH solutions on the efficiency of 30-NC/AC NC in the Pb(II) and Cd(II) adsorption. The optimal pH for the uptake of Pb(II) and Cd(II) ions was first explored by changing pH values from 2.0 to 5.0 for Pb(II) and from 3.0 to 7.0 for Cd(II). 100 mg of 30−NC/AC NC powder was dispersed in 100 mL of metal ions (100 ppm) for 120 min. Overall, the Pb(II) and Cd(II) removal percentage at low pH (2) was 60.98 and 58.76%, respectively. This decrease in % removal of toxic metal ions is due to the electrostatic repulsion of positive metal ions with excess formed protons (H^+) on the adsorbent. In addition, it can attribute the decrease in % removal of metal ions at low pH conditions (pH = 2) to the occurrence of Cu or Ni ion leaching. While the solution pH was increased (by 2.0 M NaOH), the % removal of metal ions increased and it was 100% at pH 5 for Pb(II) and 99.86% at pH 7 for Cd(II) ions. Therefore, it can be concluded that complete removal has occurred especially for lead ions. Upon increasing the solution pH above 5.0 for Pb(II), and 7.0 for Cd(II), the onset of Cd(II) and Pb(II) precipitation was observed, indicating the formation of M−OH which leads to uncertainty concerning adsorption.[32] The increase in the removal percentage with increasing pH could be explained by the deprotonation of adsorbent surfaces, so the electrostatic attractions between the adsorbent surface and pollutant ions become very low.

3.2.2. Effect of Initial Metal Ion Concentration. The effect of Cd(II) and Pb(II) concentration on the adsorptive performance of the 30-NC/AC NC adsorbent (Figure 7) revealed that as the initial concentration increased from 30 to 220 mg/L, the % removal decreased from 100% (at 30 ppm) to 83.09% (at 220 ppm) for Pb(II) and to 81.78% (at 220 ppm) for Cd(II), respectively. As metal ion concentrations increased, the repulsive forces between free pollutant ions and adsorbed pollutant ions increased. It can be concluded that complete removal has occurred with low initial concentrations (30−100 ppm), so in the present study, 100 ppm metal ion concentration was selected for the effective adsorption of heavy-metal ions from water. The decreasing % removal with increasing initial pollutant ion concentration (above 100 ppm) may be attributed to the fact that fabricated adsorbents have become saturated at high initial concentrations.

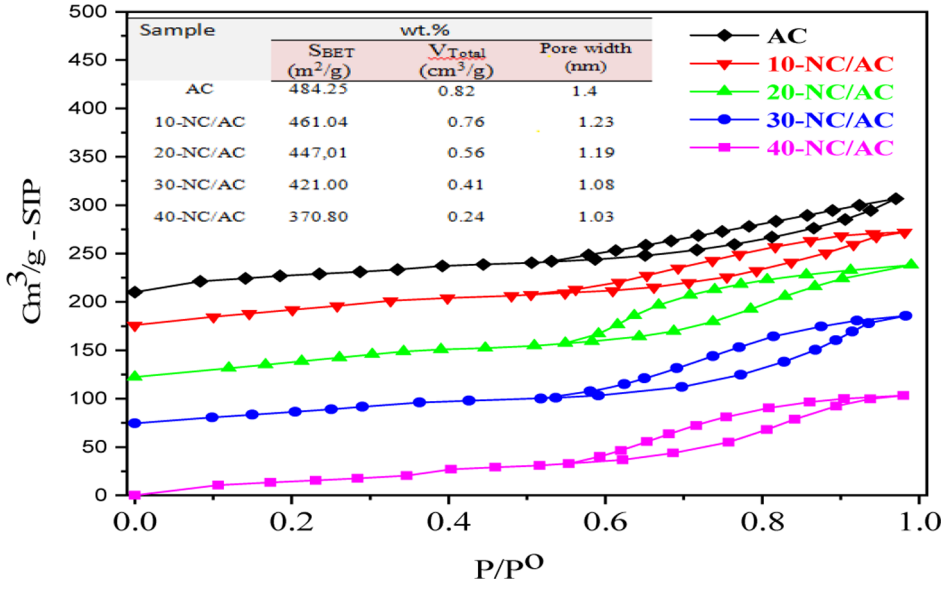

Figure 5. N_2 adsorption/desorption isotherms of pure-AC, 10-NC/AC NC, 20-NC/AC NC, 30-NC/AC NC, and 40-NC/AC NC samples.

https://doi.org/10.1021/acsomega.2c06352
ACS Omega 2022, 7, 47183−47191

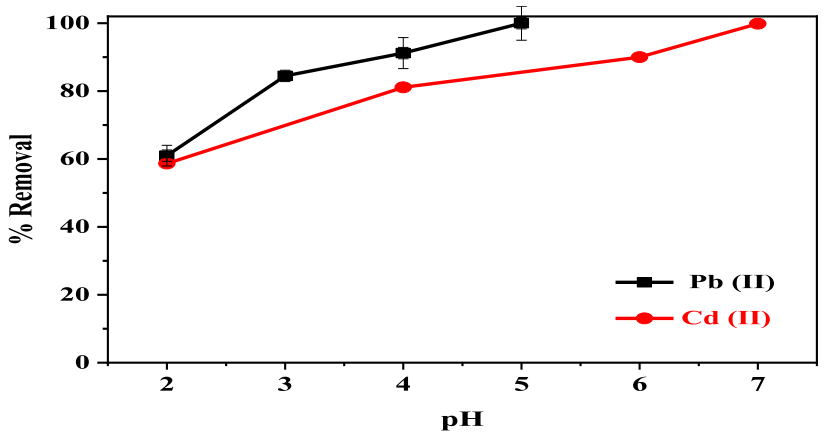

Figure 6. Effect of the solution pH on the removal of Pb(II) and Cd(II) ions from water.

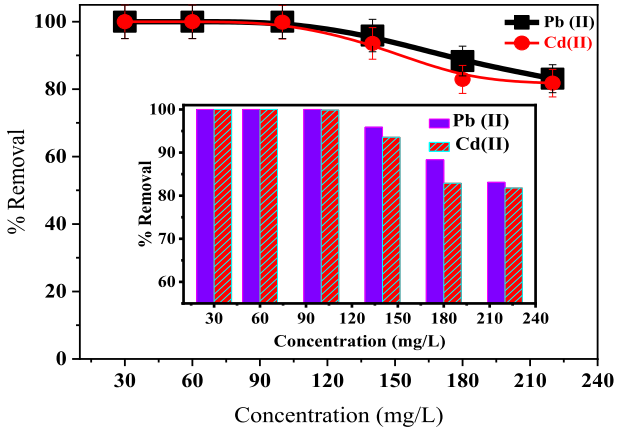

Figure 7. Effect of initial metal ion concentration on the removal of Pb(II) and Cd(II) ions.

Figure 8a,b shows the Freundlich and Langmuir isotherms for Pb(II), and Cd(II) adsorption onto the *x*-NC/AC NC. The competition for the adsorption surface site increases along with the increase of Pb(II) and Cd(II) concentrations and the sorption surface sites on the *x*-NC/AC NC limit. Therefore, the sorption rates decrease with the increase of the Pb(II) and Cd(II) concentrations. Figure 7a,b shows satisfactory linear plots, indicating the fitting of the Pb(II) and Cd(II) adsorption data to the Langmuir equation. The Freundlich and Langmuir constants as determined from the linear adsorption isotherms plots, together with corresponding values of R^2, are listed in Table 1. Based on the obtained R^2, it has been concluded that the Langmuir model gives a better fitting result than the Freundlich model. From the Langmuir model, it was observed that the obtained R^2 values were 0.991 and 0.990 for Pb(II) and Cd(II), respectively, showing that the adsorption of Pb(II) and Cd(II) onto *x*-NC/AC NC adsorbents was favorable. From the Freundlich isotherm, the *n* values were 10.0 and 9.89 for Pb(II) and Cd(II), respectively, which prove that adsorption is favorable and the process is physical in nature. Table 2 compares the adsorption capacities of different adsorbents for Pb(II) and Cd(II) ions to the 30-NC/AC NC adsorbent. According to the adsorption results, the modified 30-NC/AC NC adsorbent outperformed the other adsorbents.[34−38]

3.2.3. Effect of the Adsorbent Dose. The effect of *x*-NC/AC NC dosage on adsorption was studied using different dosages ranging from 30 to 140 mg of the 30-NC/AC NC adsorbent (Figure 9). Adsorption efficiency is highly dependent on the adsorbent amount added, according to the results. The maximum removal rates for lead (100 mg/L, 100 ml) and cadmium (100 mg/L, 100 mL) were 100 and 99.89%, respectively, using 100 mg of the adsorbent. When the adsorbent concentration increased, more surfaces or "surface

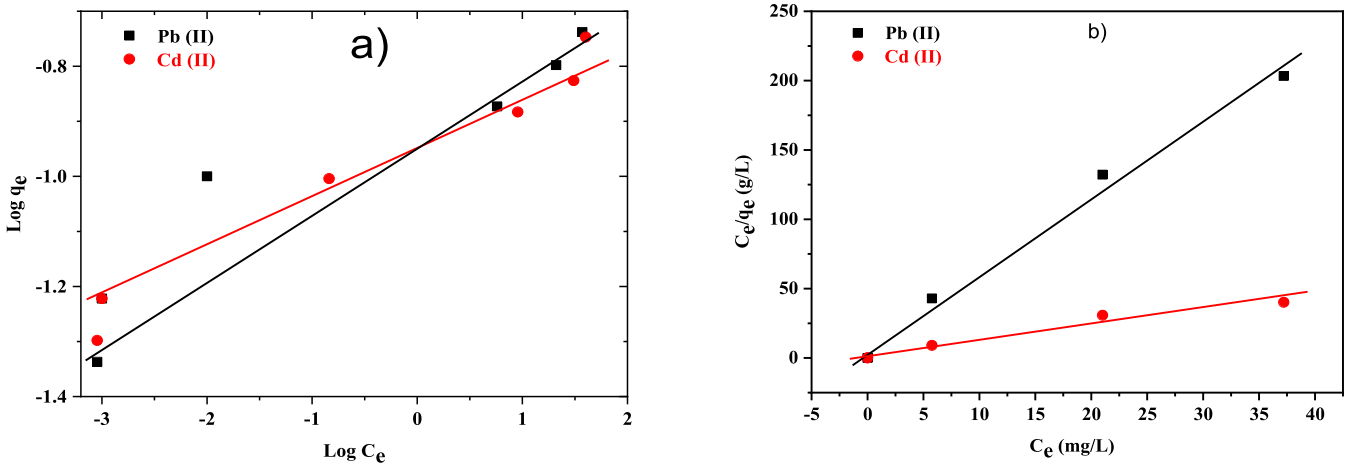

Figure 8. (a) Freundlich and (b) Langmuir isotherms for Pb(II) and Cd(II) adsorption onto the 30-NC/AC NC adsorbent.

https://doi.org/10.1021/acsomega.2c06352
ACS Omega 2022, 7, 47183−47191

Table 1. Adsorption Isotherm Parameters of Cd(II) and Pb (II)G onto the 30-NC/AC NC Adsorbent

		Langmuir isotherm				Freundlich isotherm		
adsorbent 30-NC/AC NC	q_{m}exp (mg g^{-1})	q_{m}calcd (mg g^{-1})	KL (L g^{-1})	R_L	R^2	K_f((mg g^{-1})/(mg $mL^{-1})^{1/n}$)	n	R^2
Pb(II)	182.78	176.99	1.12	0.0023	0.991	58.98	10.0	0.949
Cd(II)	179.92	166.66	1.01	0.0022	0.990	47.70	9.87	0.965

Table 2. Maximum Adsorption Capacities q_m (mg/g) of Pb(II) and Cd(II) Ions Using Various Adsorbents

adsorbent	Pb(II) q_m(mg/g)	Cd(II) q_m(mg/g)	refs
AC/pyrolusite (ACP)	66.14	7.55	34
Fe_3O_4@SiO_2−NH_2/GO NC	13.46	18.58	35
SiO_2−NH-HPBT	68.6	24.7	36
CuO NPs	88.80	15.60	37
rGO-PDTC/Fe_3O_4 NC	147.06	116.28	38
30-NC/AC NCs	182.78	179.92	this work

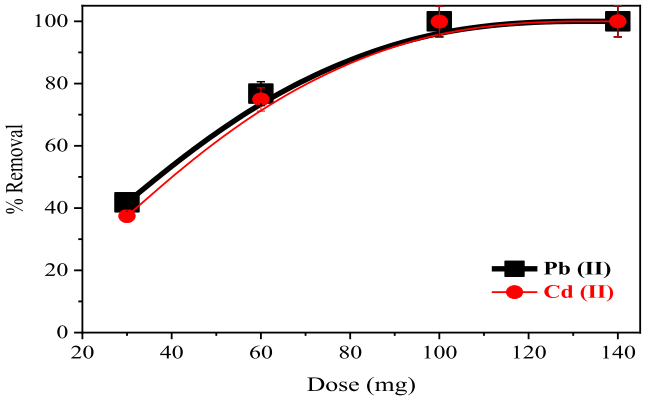

Figure 9. Effect of adsorbent dosage on the removal of Pb(II) and Cd(II) ions.

active sites" became available for pollutant ion adsorption. The completed % removal of pollutant ions at 100 mg of the nanoadsorbent or more doses could be attributed to the increase of the surface area and surface active sites with an increase in the adsorbent NPs, leading to enhancement of the adsorptive performance of *x*-NC/AC NC adsorbents. As a result, the optimal dosage to obtain completed removal was 100 mg and more. Therefore, in the present study, 100 mg of *x*-NC/AC NC adsorbents was selected for the effective adsorption of Pb(II) and Cd(II) ions.

3.2.4. Effect of Contact Time and the Kinetic Study. The effect of contact time on the removal of Pb(II) and Cd(II) is shown in Figure 10a,b. The results showed that both metal ions had relatively fast-high adsorption in the first 15 min. Then, the adsorption was degradingly increased after 15 min until it reached the equilibrium state at 30 min, and then % removal was constant with an increase in time to 120 min. The maximum % removal after 30 min was 90.01, 93.20, 96.45, 100, and 96.93% for Pb(II) and 89.56, 92.10, 95.99, 99.89, and 94.89% using pure-AC, 10-NC/AC, 20-NC/AC, 30-NC/AC, and 40-NC/AC NC adsorbents, respectively. The highest % removal was 100% for Pb(II), and 99.89% for Cd(II) using the 30-NC/AC NC adsorbent within 30 min, which was optimum. The experimental adsorption results showed that the adsorptive performance of the 10-, 20-, 30-, and 40-NC/AC NC adsorbents was greatly enhanced after loading hybrid NiO−CuO NPs. This may be due to more functional Cu−O

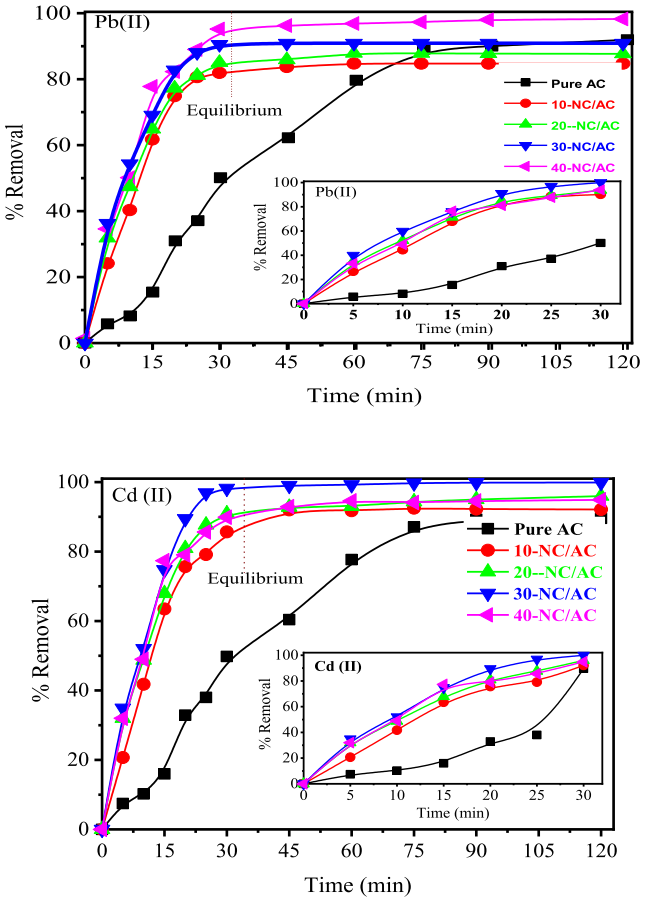

Figure 10. Effect of contact time on the removal of Pb(II) and Cd(II) ions.

and Ni−O groups attached to the AC structure being available to bind more metallic pollutants. The enhanced adsorptive performance of fabricated *x*-NC/AC NC adsorbents may be due to the increase in the active sites on the AC surface, which can be concluded by decreasing the specific surface area from 484.25 m^2/g for the pure-AC adsorbent to 370.80 m^2/g for the 40-NC/AC NC adsorbent. This decrease in the surface area, pore volume, and diameter proves the increase in the hybrid active sites on the x-NC/AC NCs surfaces, as confirmed by FE-SEM images. The decreasing % removal with the 40-NC/AC NC adsorbent may be due to some clumps formed on this adsorbent surface with the increase of the loaded nanohybrid NiO−CuO on the AC surface above 30 wt %, which led to a decrease in the removal percentage with a significant decrease in the surface area of the 40-NC/AC NC adsorbent (370.80 m^2/g).

The adsorption kinetics behavior of Pb(II) and Cd(II) adsorption onto the surface of NC/AC NC adsorbents was studied and explained by two models. These kinetic equations include the pseudo-first-order and pseudo-second-order models. Figure 11 shows the pseudo-first-order kinetics and

https://doi.org/10.1021/acsomega.2c06352
ACS Omega 2022, 7, 47183−47191

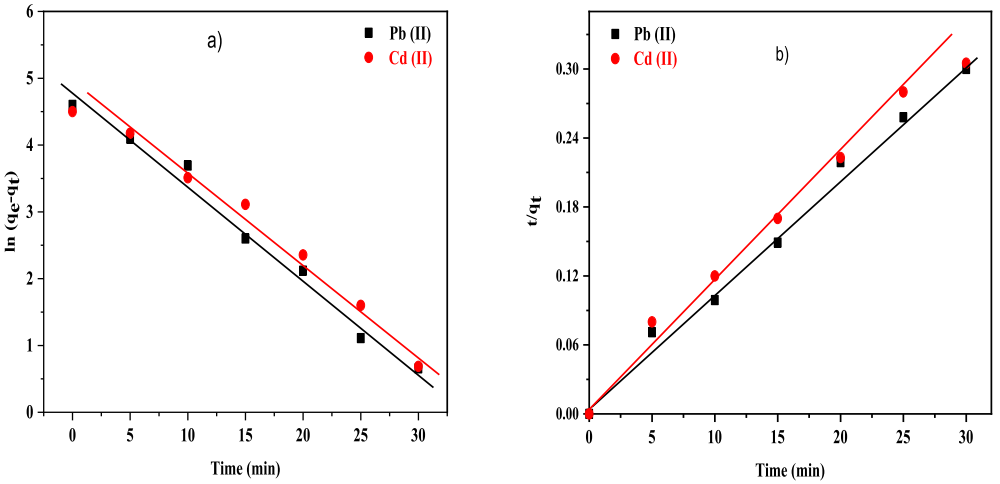

Figure 11. (a) Pseudo-first-order kinetics and (b) pseudo-second-order kinetics for Pb(II) and Cd(II) adsorption onto the 30-NC/AC NC adsorbent.

pseudo-second-order kinetics for Pb(II) and Cd(II) adsorption onto the *x*-NC/AC NC adsorbents. Table 1 lists the detailed model fitting data about these models. In general, the R^2 (correlation coefficients) was used to test the accuracy of the models. The relatively higher R^2 value manifests that the Pb(II), and Cd(II) adsorption processes described by this model are applicable and the obtained fitting parameters are reliable. Among the two models, the R^2 value of the pseudo-second-order kinetics is the largest, and the error between experimental values (qe, exp) and (qe, cal) is little. Therefore, the Pb(II) and Cd(II) adsorption processes are the most appropriate explained by the pseudo-second-order kinetics.

3.2.5. Effect of Recycling of x-NC/AC NC Adsorbents. The effect of reusing fabricated *x*-NC/AC NC adsorbents on the adsorption of Pb(II) and Cd(II) ions using 100 mg of the 30-NC/AC NC adsorbent is shown in Figure 12. The % removal of lead and cadmium ions was very slightly reduced with reusing, from 100 and 99.89% of the first use to about 98.52 and 98.02% of the fourth reuse for Pb(II) and Cd(II) ions, respectively. This demonstrates that the prepared *x*-NC/AC NCs are efficient stable adsorbents after four reuses. The slight decrease in % removal may be due to the presence of chloride ions originating from the metal salt or the gradual loss of weight of the *x*-NC/AC NCs during filtration and washing.[33] According to our recyclability study results, the fabricated *x*-NC/AC NC adsorbents can be used as effective and reliable adsorbents in water treatment repetitively.

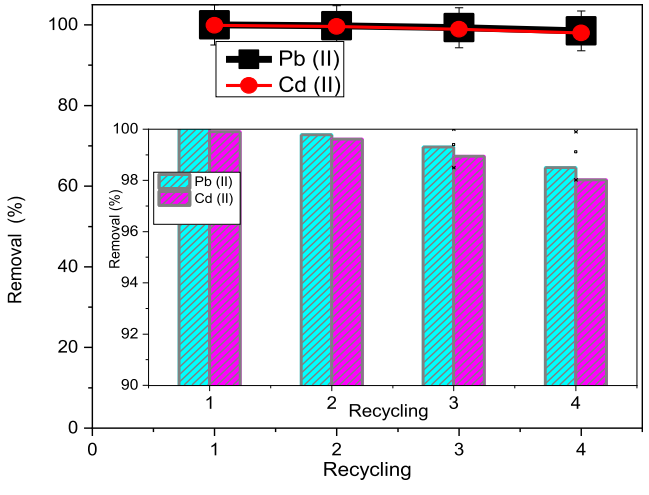

Figure 12. Effect of adsorbent recycling on the removal of Pb(II) and Cd(II) ions from water.

3.2.6. Effect of Coexisting Pb and Cd Ions on the Adsorption Process. It was necessary to determine the effect of coexisting metal ions and competitive adsorption when considering the adsorption of Cd(II) and Pb(II) ions. The adsorption results are given in Figure 13. The % removal of Pb (II) from the binary system was 95.23%, and the % removal of Pb(II) from the binary system was 92.01%; the average % removal of both Pb(II) and Cd(II) ions was 93.62%. It was apparent that the % removal of both Pb(II) and Cd(II) ions in the binary system was slightly lower (little deference) than that of each heavy-metal ion adsorbed alone. The % removal of Pb(II) was higher than the % removal of Cd(II). When Pb(II) and Cd(II) coexisted, the % removal of Pb(II) was a little preferable for the adsorbent. Compared with the % removal of Cd(II), the % removal of Pb(II) was slightly higher than the % removal of Cd(II) ions. This is due to the similar structure of Pb^{2+} and Cd^{2+} ions. The relatively small hydrated ionic radius of Pb^{2+} ions makes it more easily to compete with Cd^{2+} ions for adsorption sites, and Pb^{2+} ions can rapidly bind to the active functional groups on the NC/AC NC adsorbent. The results further show that although the competitive effect reduced the % removal of both Pb(II) and Cd(II) ions, there was preferential adsorption for Pb(II) ions. This work may also provide some new applications for the removal of Pb(II), Cd(II), and other metal ions.

4. CONCLUSIONS

This work has documented the integration of hybrid metal oxides (nanohybrid NiO−CuO) with AC material which greatly improved the adsorptive performance of fabricated adsorbents. A new series of efficient *x*-NiO-CuO/AC NC adsorbents were successfully fabricated and investigated as a key to a green environment free of hazardous metal ions. Loading hybrid NiO−CuO NPs on the AC synthesized from Arhabi-Khat leaves (as a plant source in Yemen) was successfully performed and confirmed using different characterization techniques. The fabricated 30-NiO-CuO/AC NC adsorbent exhibited nearly complete removal of Pb(II) and

https://doi.org/10.1021/acsomega.2c06352
ACS Omega 2022, 7, 47183−47191

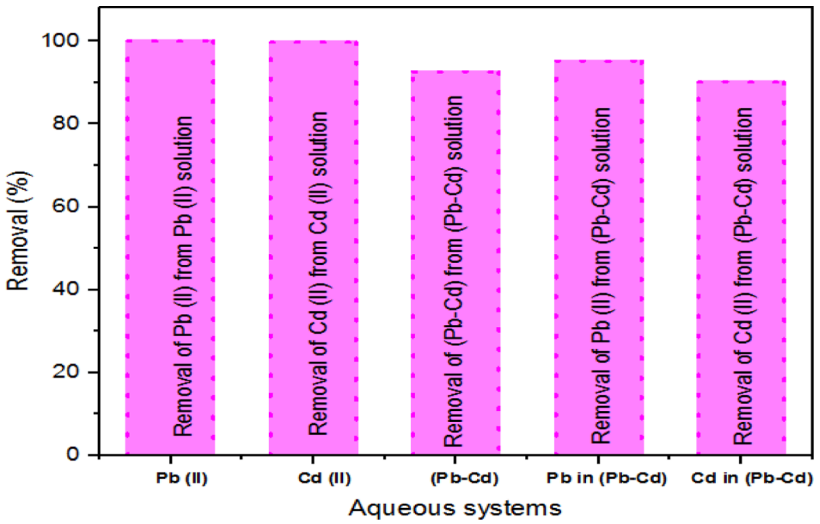

Figure 13. Effect of coexisting Pb and Cd ions on the adsorption process.

Cd(II), efficiently recycled several times. The obtained superior adsorption results showed that hybrid NiO−CuO NPs enhanced the adsorptive performance of the AC material, showing a bright future for its application in water treatment. Therefore, chemical researchers should do more follow-up work to evaluate other mixed metal oxides loaded on AC materials and their application in water treatment.

AUTHOR INFORMATION

Corresponding Author

Fares T. Alshorifi − *Department of Chemistry, Faculty of Science, Sana'a University, Sana'a 72738, Yemen; Department of Chemistry, Faculty of Science, University of Saba Region, Mareb 761107, Yemen;* orcid.org/0000-0002-2818-9613; Email: amgdfaress@gmail.com, F.Alshareefi@su.edu.ye

Authors

Bara'ah Yahya Hashem − *Department of Chemistry, Faculty of Education, Sana'a University, Sana'a 72738, Yemen*

Abdullah A. Alswat − *Department of Chemistry, Faculty of Education and Applied Science-Arhab Sana'a University, Sana'a 72738, Yemen*

Shaimaa L. Ali − *Department of Chemistry, Faculty of Science, Mansoura University, Mansoura 002, Egypt*

Najat A. Al-Odaini − *Department of Chemistry, Faculty of Science, Sana'a University, Sana'a 72738, Yemen*

Complete contact information is available at: https://pubs.acs.org/10.1021/acsomega.2c06352

Notes

The authors declare no competing financial interest.

ACKNOWLEDGMENTS

This work was supported by the authors.

REFERENCES

(1) Ibrahim, A. A.; Ali, S. L.; Adly, M. S.; El-Hakam, S.; Samra, S.; Ahmed, A. I. Green construction of eco-friendly phosphotungstic acid Sr-MOF catalysts for crystal violet removal and synthesis of coumarin and xanthene compounds. *RSC Adv.* **2021**, *11*, 37276−37289.

(2) Fu, F.; Wang, Q. Removal of heavy metal ions from wastewaters: a review. *J. Environ. Manage.* **2011**, *92*, 407−418.

(3) Mishra, S.; Bharagava, R. N.; More, N.; Yadav, A.; Zainith, S.; Mani, S.; Chowdhary, P.Heavy metal contamination: an alarming threat to environment and human health. In *Environmental biotechnology: For sustainable future*, 1st ed.; Sobti, R., Arora, N., Kothari, R., Eds.; Springer: Singapore, 2019; pp 103−125.

(4) Ning, C.-c.; Gao, P.-d.; Wang, B.-q.; Lin, W.-p.; Jiang, N.-h.; Cai, K.-z. Impacts of chemical fertilizer reduction and organic amendments supplementation on soil nutrient, enzyme activity and heavy metal content. *J. Integr. Agric.* **2017**, *16*, 1819−1831.

(5) Engwa, G. A.; Ferdinand, P. U.; Nwalo, F. N.; Unachukwu, M. N.Mechanism and health effects of heavy metal toxicity in humans. *Poisoning in the modern world-new tricks for an old dog*, 2nd ed.; Karcioglu, O., Arslan, B., Eds.; IntechOpen: London, 2019; pp 70−90.

(6) Du, B.; Zhou, J.; Lu, B.; Zhang, C.; Li, D.; Zhou, J.; Jiao, S.; Zhao, K.; Zhang, H. Environmental and human health risks from cadmium exposure near an active lead-zinc mine and a copper smelter, China. *J. Sci. Total Environ.* **2020**, *720*, 137585.

(7) Latif, J.; Akhtar, J.; Ahmad, I.; Mahmood-ur-Rehman, M.; Shah, G. M.; Zaman, Q.; Javaid, T.; Farooqi, Z. U. R.; Shakar, M.; Saleem, A.; Rizwan, M. Unraveling the effects of cadmium on growth, physiology and associated health risks of leafy vegetables. *Braz. J. Rev. Bras. Bot.* **2020**, *43*, 799−811.

(8) Saini, S.; Dhania, G.Cadmium as an environmental pollutant: ecotoxicological effects, health hazards, and bioremediation approaches for its detoxification from contaminated sites. In *Bioremediation of industrial waste for environmental safety*, 2nd ed.; Bharagava, R., Saxena, G., Eds.; Springer: Singapore, 2020; pp 357−387.

(9) Shahriar, S.; Rahman, M. M.; Naidu, R. Geographical variation of cadmium in commercial rice brands in Bangladesh: Human health risk assessment. *J. Sci. Total Environ.* **2020**, *716*, 137049.

(10) Suhani, I.; Sahab, S.; Srivastava, V.; Singh, R. P. Impact of cadmium pollution on food safety and human health. *J. Curr. Opin. Toxicol.* **2021**, *27*, 1−7.

(11) Assi, M. A.; Hezmee, M. N. M.; Haron, M. Y. M.; Sabri, M. A.; Rajion, M. A. The detrimental effects of lead on human and animal health. *J. Vet. World.* **2016**, *9*, 660.

(12) Samarghandian, S.; Shirazi, F. M.; Saeedi, F.; Roshanravan, B.; Pourbagher-Shahri, A. M.; Khorasani, E. Y.; Farkhondeh, T.; Aaseth, J. O.; Abdollahi, M.; Mehrpour, O. A systematic review of clinical and laboratory findings of lead poisoning: lessons from case reports. *J. Toxicol. Appl. Pharmacol.* **2021**, *429*, 115681.

(13) Gunatilake, S. Methods of removing heavy metals from industrial wastewater. *J. Multidiscip. Eng. Sci. Stud.* **2015**, *1*, 14.

(14) Iro, Z. S.; Subramani, C.; Dash, S. A brief review on electrode materials for supercapacitor. *Int. J. Electrochem. Sci.* **2016**, *11*, 10628−10643.

(15) Zhang, W.; Cheng, H.; Niu, Q.; Fu, M.; Huang, H.; Ye, D. Microbial targeted degradation pretreatment: a novel approach to preparation of activated carbon with specific hierarchical porous structures, high surface areas, and satisfactory toluene adsorption performance. *J. Environ. Sci. Technol.* **2019**, *53*, 7632−7640.
(16) Ge, H.; Wang, J. Ear-like poly (acrylic acid)-activated carbon nanocomposite: A highly efficient adsorbent for removal of Cd (II) from aqueous solutions. *J. Chemosphere.* **2017**, *169*, 443−449.
(17) Larsson, P.-O.; Andersson, A. Complete oxidation of CO, ethanol, and ethyl acetate over copper oxide supported on titania and ceria modified titania. *J. Catal.* **1998**, *179*, 72−89.
(18) Chikán, V.; Molnár, Á.; Balázsik, K. One-step synthesis of methyl isobutyl ketone from acetone and hydrogen over Cu-on-MgO catalysts. *J. Catal.* **1999**, *184*, 134−143.
(19) Richardson, J. T. Surface properties of nickel oxide. *J. Catal.* **1966**, *6*, 328−332.
(20) Flevet, F.; Flglarz, M. Preparation and study by electron microscopy of the development of texture with temperature of a porous exhydroxide nickel oxide. *J. Catal.* **1975**, *39*, 350−356.
(21) Kaur, J.; Kaur, M.; Ubhi, M. K.; Kaur, N.; Greneche, J.-M. Composition optimization of activated carbon-iron oxide nanocomposite for effective removal of Cr (VI) ions. *J. Mater. Chem. Phys.* **2021**, *258*, 124002.
(22) Jain, M.; Yadav, M.; Kohout, T.; Lahtinen, M.; Garg, V. K.; Sillanpää, M. Development of iron oxide/activated carbon nanoparticle composite for the removal of Cr (VI), Cu (II) and Cd (II) ions from aqueous solution. *J. Water Resour. Ind.* **2018**, *20*, 54−74.
(23) Kakavandi, B.; Kalantary, R. R.; Farzadkia, M.; Mahvi, A. H.; Esrafili, A.; Azari, A.; Yari, A. R.; Javid, A. B. Enhanced chromium (VI) removal using activated carbon modified by zero valent iron and silver bimetallic nanoparticles. *J. Environ. Health. Sci. Engineer.* **2014**, *12*, 1−10.
(24) Alhan, S.; Nehra, M.; Dilbaghi, N.; Singhal, N. K.; Kim, K.-H.; Kumar, S. Potential use of ZnO@ activated carbon nanocomposites for the adsorptive removal of Cd^{2+} ions in aqueous solutions. *J. Environ. Res.* **2019**, *173*, 411−418.
(25) Yadav, M. S.; Singh, N.; Bobade, S. M. Electrochemical analysis of CuO-AC based nanocomposite for supercapacitor electrode application. *J. Mater. Today: Proc.* **2020**, *28*, 366−374.
(26) Hammani, H.; Boumya, W.; Laghrib, F.; Farahi, A.; Lahrich, S.; Aboulkas, A.; El Mhammedi, M. Electrocatalytic effect of NiO supported onto activated carbon in oxidizing phenol at graphite electrode: application in tap water and olive oil samples. *J. Assoc. Arab Univ. Basic Appl. Sci.* **2017**, *24*, 26−33.
(27) Kaipannan, S.; Marappan, S. Fabrication of 9.6 V high-performance asymmetric supercapacitors stack based on nickel hexacyanoferrate-derived $Ni(OH)_2$ nanosheets and bio-derived activated carbon. *Sci. Rep.* **2019**, *9*, 1104.
(28) Zahariev, I.; Piskin, M.; Karaduman, E.; Ivanova, D.; Markova, I.; Fachikov, L.FTIR spectroscopy method for investigation of Co-Ni nanoparticle nanosurface phenomena. *J. Chem. Technol. Metall.***2017**, *52* ().
(29) Wang, J.; Chen, J.; Peng, L.; Zhang, H.; Jiang, Z.; Xiong, K.; Yang, Q.; Chen, J.; Yang, N. On the CuO-Mn_2O_3 oxide-pair in $CuMnO_x$ multi-oxide complexes: Structural and catalytic studies. *J. Appl. Surf. Sci.* **2022**, *575*, 151−733.
(30) Li, S.-J.; Xia, N.; Lv, X.-L.; Zhao, M.-M.; Yuan, B.-Q.; Pang, H. A facile one-step electrochemical synthesis of graphene/NiO nanocomposites as efficient electrocatalyst for glucose and methanol. *J. ens. Actuators B Chem.* **2014**, *190*, 809−817.
(31) Khatamian, M.; Divband, B.; Shahi, R. Ultrasound assisted co-precipitation synthesis of Fe_3O_4/bentonite nanocomposite: performance for nitrate, BOD and COD water treatment. *J. Water Process. Eng.* **2019**, *31*, 100−870.
(32) Zhou, N.; Chen, H.; Xi, J.; Yao, D.; Zhou, Z.; Tian, Y.; Lu, X. Biochars with excellent Pb (II) adsorption property produced from fresh and dehydrated banana peels via hydrothermal carbonization. *J. Bioresour. Technol.* **2017**, *232*, 204−210.
(33) Masindi, V.; Gitari, W. Simultaneous removal of metal species from acidic aqueous solutions using cryptocrystalline magnesite/bentonite clay composite: an experimental and modelling approach. *J. Clean. Prod.* **2016**, *112*, 1077−1085.
(34) Xie, R.; Jiang, W.; Wang, L.; Peng, J.; Chen, Y. Effect of pyrolusite loading on sewage sludge-based activated carbon in Cu (II), Pb (II), and Cd (II) adsorption. *J. Environ. Prog. Sustain. Energy.* **2013**, *32*, 1066−1073.
(35) Donga, C.; Mishra, S. B.; Abd-El-Aziz, A. S.; Ndlovu, L. N.; Mishra, A. K.; Kuvarega, A. T. (3-Aminopropyl) Triethoxysilane (APTES) Functionalized Magnetic Nanosilica Graphene Oxide (MGO) Nanocomposite for the Comparative Adsorption of the Heavy Metal [Pb (II), Cd (II) and Ni (II)] Ions from Aqueous Solution. *J. Inorg. Organomet. Polym. Mater.* **2022**, *32*, 2235−2248.
(36) Güçoğlu, M.; Şatıroğlu, N. Adsorption of Pb (II), Cu (II), Cd (II), Ni (II), and Co (II) ions by newly synthesized 2-(2′-Hydroxyphenyl) Benzothiazole-functionalized silica. *J. Mol. Liq.* **2022**, *348*, 118−388.
(37) Mahmoud, A. E. D.; Al-Qahtani, K. M.; Alflaij, S. O.; Al-Qahtani, S. F.; Alsamhan, F. A. Green copper oxide nanoparticles for lead, nickel, and cadmium removal from contaminated water. *Sci. Rep.* **2021**, *11*, 1−13.
(38) Fu, W.; Huang, Z. Magnetic dithiocarbamate functionalized reduced graphene oxide for the removal of Cu (II), Cd (II), Pb (II), and Hg (II) ions from aqueous solution: Synthesis, adsorption, and regeneration. *Chemosphere* **2018**, *209*, 449−456.

https://doi.org/10.1021/acsomega.2c06352
ACS Omega 2022, 7, 47183−47191